Chemical Science

ROYAL SOCIETY OF CHEMISTRY

EDGE ARTICLE

View Article Online
View Journal | View Issue

Cite this: *Chem. Sci.*, 2025, **16**, 18791

All publication charges for this article have been paid for by the Royal Society of Chemistry

Received 15th July 2025
Accepted 4th September 2025

DOI: 10.1039/d5sc05270j

rsc.li/chemical-science

Dynamic networks of fluorine-rich acrylates enable highly conductive and flame-retardant electrolytes for lithium metal batteries

Junyi Gan,[a] Yao Zhao,[a] Zhan Jiang,[a] Chenyu Yang,[a] Da Ke,[a] Qichao Wang,*[a] Ye Liu,*[b] Xiaohui Zeng*[c] and Tengfei Zhou*[a]

A fluorinated gel polymer electrolyte (FGPE) was synthesized *via in situ* copolymerization of acrylamide (AM) and 1, 1, 1, 3, 3, 3-hexafluoroisopropyl acrylate (HFA). The synergistic interaction between $-CF_3$ and C=O groups endows the electrolyte with high ionic conductivity (1.21×10^{-3} S cm^{-1}), a lithium-ion transference number of 0.68, and an electrochemical stability window up to 4.75 V. Symmetric Li||FGPE||Li cells exhibit stable cycling for over 1000 hours with a polarization voltage of 25 mV. Meanwhile, LFP||Li full cells retain 87% of their initial capacity after 200 cycles, confirming the effectiveness of synergistic interactions between $-CF_3$ and C=O in enhancing the performance of high-energy lithium metal batteries. This study establishes a design paradigm for high-conductivity functional gel polymer electrolytes, providing a viable pathway toward lithium metal batteries with integrated high stability and high conductivity capabilities.

The rising demand for high-energy-density batteries in multifunctional electronic products and appliances for extreme environment scenarios has positioned lithium metal batteries (LMBs) as promising candidates due to their ultrahigh theoretical capacity (3860 mA h g^{-1}) and the lowest electrochemical potential (−3.04 V *vs.* SHE).[1–4] However, the flammability of conventional liquid electrolytes and uncontrolled lithium dendrite growth significantly limit their commercial viability.[5,6] Solid-state/gel polymer electrolytes (GPEs), with their non-flammable nature and mechanical flexibility, offer a compelling alternative. However, an ideal GPE must achieve high ionic conductivity (>10^{-3} S cm^{-1}), a wide electrochemical stability window (>4.5 V *vs.* Li$^+$/Li), and excellent compatibility with lithium metal interfaces.[7–10]

Traditional polymer electrolytes, such as those based on polyethylene oxide (PEO), suffer from narrow electrochemical windows (<4 V *vs.* Li$^+$/Li), making them unsuitable for high-voltage applications.[11–13] Although fluorinated polymers like PVDF-HFP extend the voltage window beyond 4.5 V, their high crystallinity leads to poor lithium-ion transport (t_{Li^+} < 0.4) and inadequate interfacial stability, resulting in heterogeneous solid electrolyte interphase (SEI) formation.[14–16] To address these challenges, recent approaches have focused on engineering multifunctional GPEs through copolymerization or blending strategies.[17] These methods introduce polar functional groups (*e.g.*, $-CONH_2$, –CN) to improve lithium salt dissociation, and fluorinated groups ($-CF_3$) to reduce HOMO energy levels and enhance oxidative stability.[18–20] Additionally, optimizing lithium salt formulations (*e.g.*, LiFSI, LiTFSI), tuning solvation structures, and employing *in situ* polymerization techniques have shown significant promise in improving ion transport and interfacial performance.[21–24]

In this work, we developed an *in situ*-formed FGPE1:1 by integrating acrylamide (AM) with fluorine-rich monomer 1, 1, 1, 3, 3, 3-hexafluoroisopropyl acrylate (HFA), dimethoxyethane (DME), initiator, lithium salt and additive to construct a dynamic fluorinated polymer network. The flexible polymer network incorporates C=O and C–F groups to establish rapid Li$^+$ transport channels, while secondary amine ($-NH_2$) groups are introduced to anchor anions, enabling high lithium salt dissociation and efficient ion transport. This design achieves superior conductivity (1.2 mS cm^{-1}), a high t_{Li^+} (0.68), and remarkable cycling performance under high current densities. The strategic inclusion of fluorine atoms facilitates the formation of fluorine-rich solid-electrolyte interphase (SEI) and cathode-electrolyte interphase (CEI) layers on both electrodes, effectively suppressing parasitic reactions between cathode particles and solvent molecules.[25] The resulting FGPE delivers a broad voltage window, high conductivity, and long-term cycling stability at ambient temperature, offering a robust strategy for designing next-generation polymer electrolytes in lithium-based energy storage systems.[26–28]

[a]*Institutes of Physical Science and Information Technology, Key Laboratory of Structure and Functional Regulation of Hybrid Material (Ministry of Education), Anhui University, Hefei 230601, China. E-mail: qcw2547@foxmail.com; tengfeiz@ahu.edu.cn*

[b]*Hubei Key Laboratory of Pollutant Analysis & Reuse Technology, College of Chemistry and Chemical Engineering, Hubei Normal University, Huangshi 435002, Hubei, China. E-mail: yliu@hbnu.edu.cn*

[c]*Institute of Surface Science, Helmholtz-Zentrum Hereon, Geesthacht 21502, Germany. E-mail: xiaohui.zeng@hereon.de*

A FGPE with an acrylamide (AM) to 1, 1, 1, 3, 3, 3-hexafluoroisopropyl acrylate (HFA) monomer molar ratio of 1 : 1 was synthesized based on a comprehensive evaluation of its ionic conductivity, mechanical properties, and cost-effectiveness (Fig. 1a). The liquid electrolyte (LE) consists of 1 M LiFSI in DME with 5 wt% FEC (purchased from Dolyan Co., Ltd). Thermal polymerization at 65 °C converted the transparent liquid precursor into a stable gel network (Fig. 1b). However, FGPE1:2 did not undergo complete gelation, and corresponding images of FGPE4:3, FGPE3:4, and FGPE1:2 before and after polymerization are provided in Fig. S1. To elucidate the antioxidant mechanisms of FGPE, we performed density functional theory (DFT) calculations (Fig. 1c and S2). These calculations show that the low LUMO energy of FEC favors its preferential reduction, yielding a LiF-rich SEI. In addition, the monomers and LiFSI have lower LUMO energies than the solvents,[29,30] which further promotes the formation of a fluorine-enriched interphase. Notably, the HOMO energies of AM (−6.82 eV) and HFA (−8.375 eV) are substantially reduced relative to that of PEO (−6.15 eV), indicating a fluorine-induced enhancement of antioxidant capacity within the polymer network.[31] This trend is consistent with the polymer's high oxidation resistance (HOMO = −7.231 eV), as corroborated by LSV measurements.[32,33] Fourier transform infrared (FTIR) spectroscopy (Fig. 1d) confirms successful polymerization, evidenced by the disappearance of the C=C stretch (1612.7 cm^{-1}) and retention of characteristic C–F vibrations (1147 cm^{-1}, 1202.98 cm^{-1}).[34,35] Complementary ^{1}H NMR data (Fig. 1e) showed the absence of the vinyl proton signal at 6 ppm,[25] while ^{13}C NMR confirmed complete consumption of the C=C bond (Fig. S3a).[36] In the ^{13}C NMR spectrum (Fig. S3a), the C=C resonances at 129.6 and 136 ppm disappear and are replaced by saturated-carbon resonances at 36 and 58.4 ppm.[37] Distinct CF_3 carbon signals at 65 and 72 ppm further corroborate the successful synthesis of FGPE1:1. The Raman spectrum of FGPE1:1 (Fig. 1f) shows three characteristic peaks at 734, 739, and 749 cm^{-1}, assigned to the free anion (uncoordinated FSI^-), a contact ion pair in which FSI^- is coordinated to one Li^+ (CIPs), and an aggregate in which FSI^- is coordinated to two or more Li^+ (AGG), respectively.[38] It reveals predominantly AGG and CIP species of FGPEs, indicating strong Li^+–FSI^- interactions. FGPE1:1 exhibits a greater presence of CIP and AGG structures compared to FGPE1:2, indicating a weakened Li^+ solvation ability.[39] This coordination environment promotes the formation of CIPs and AGGs, which in turn facilitates Li^+ transport and contributes to the stabilization of the lithium metal[40] anode and the excess free fluorine content is shown to be detrimental to lithium ion migration. Furthermore, the polymer matrix appears to stabilize these ionic aggregates while reducing Li^+ solvation capacity, likely due

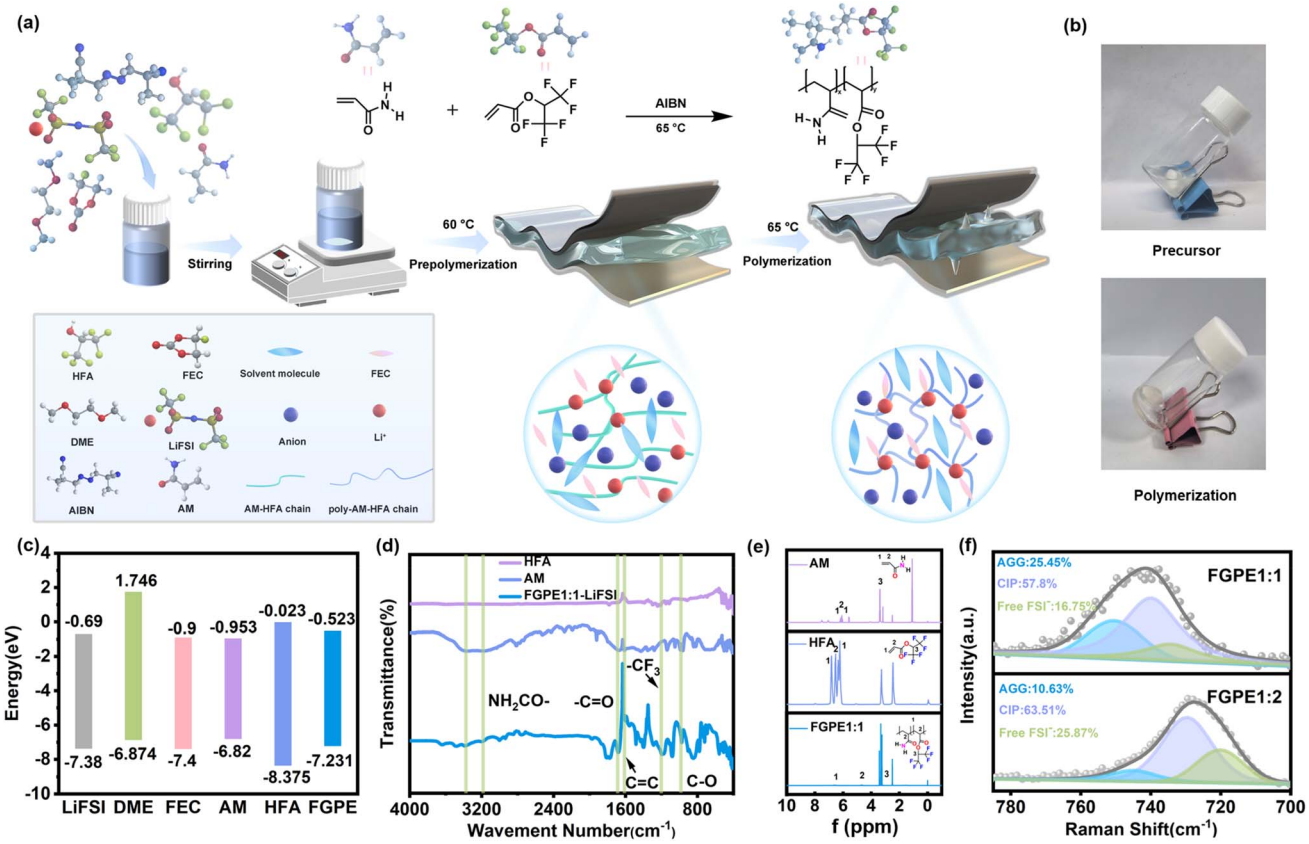

Fig. 1 (a) Flowchart of the preparation of the fluorinated gel polymer electrolyte. (b) Photographs of the FGPE before and after polymerization. (c) Calculated LUMO and HOMO energy values of the main components of DME, FEC, AM and HFA based on density functional theory. (d) FTIR spectra of monomers and FGPEs. (e) ^{1}H liquid-state NMR spectra of AM, HFA and FGPE1:1. (f) Raman spectra of FGPE1:1 and FGPE1:2.

to weakened Li^+–O interactions induced by ester functional groups.[15]

The long-term cycling stability of Li||FGPE||Li symmetric cells was evaluated on Neware battery test system (CT-4008Tn-5V20mA-HWX) at 0.1 mA cm^{-2} with a capacity of 0.1 mA h cm^{-2} (Fig. 2a). The Li||FGPE4:3||Li cell short-circuited after 70 h, likely due to the excessive free AM content, which increased polymer rigidity and interfacial impedance, thereby hindering impaired Li^+ transport kinetics. In contrast, Li||FGPE1:1||Li exhibited exceptional stability, maintaining a low overpotential (~25 mV) for over 1000 h, whereas Li||FGPE1:2||Li and Li||liquid electrolyte (LE)||Li failed after 224 h. The LE cell showed severe voltage fluctuations (peaking at 100 mV) before failure at 381 h due to dendrite penetration. To assess the ability of FGPE1:1 to suppress lithium dendrite growth, we examined the surface morphology of lithium metal anodes after 100 cycles in Li||FGPE1:1||Li and Li||FGPE1:2||Li cells using scanning electron microscopy (SEM) (Fig. 2b). FGPE1:1 facilitated uniform Li deposition (Fig. 2b), in contrast to FGPE1:2, which remained in a gel state. Furthermore, FGPE1:1 formed a thinner solid electrolyte interphase (SEI) (~5 nm) compared to FGPE1:2 (~20 nm, Fig. S4), with energy-dispersive X-ray spectroscopy (EDS) mapping confirming homogeneous fluorine distribution (Fig. S6a). The Li||FGPE1:1||Li cell demonstrated stable cycling for 470 h at a current density of 0.3 mA cm^{-2} and a capacity of 0.3 mA h cm^{-2} (Fig. S7a), highlighting superior Li plating/stripping behavior and dendrite suppression. Additionally, FGPE1:1 exhibited outstanding rate capability, maintaining polarization below 0.2 mV across current densities of 0.05–1 mA cm^{-2} (Fig. S7b). As shown in Fig. 2c, LFP||FGPE1:1||Li delivered the highest initial discharge capacity (151.54 mA h g^{-1}) and coulombic efficiency (96.91%), retaining 99.81% capacity after 70 cycles, significantly outperforming LE (70.86%, 113.22 mA h g^{-1}). FGPE1:2 demonstrated the poorest capacity retention, with its discharge capacity declining from 118.71 mA h g^{-1} to 70.5 mA h g^{-1}, with a coulombic efficiency of 81.97%. Fig. S7c displays the coulombic efficiencies of different types of FGPEs and LE at a current density of 0.2C. As demonstrated in Fig. 2d, LFP||FGPE1:1||Li maintained 87% capacity retention after 200 cycles at 0.2C. At 0.5C, FGPE1:1 retained 85.5% capacity after 400 cycles (Fig. S7d), attributed to its high ionic conductivity, which reduces internal resistance and enhances rate performance. Among the tested FGPE ratios, FGPE1:1 delivers the highest initial specific capacity and

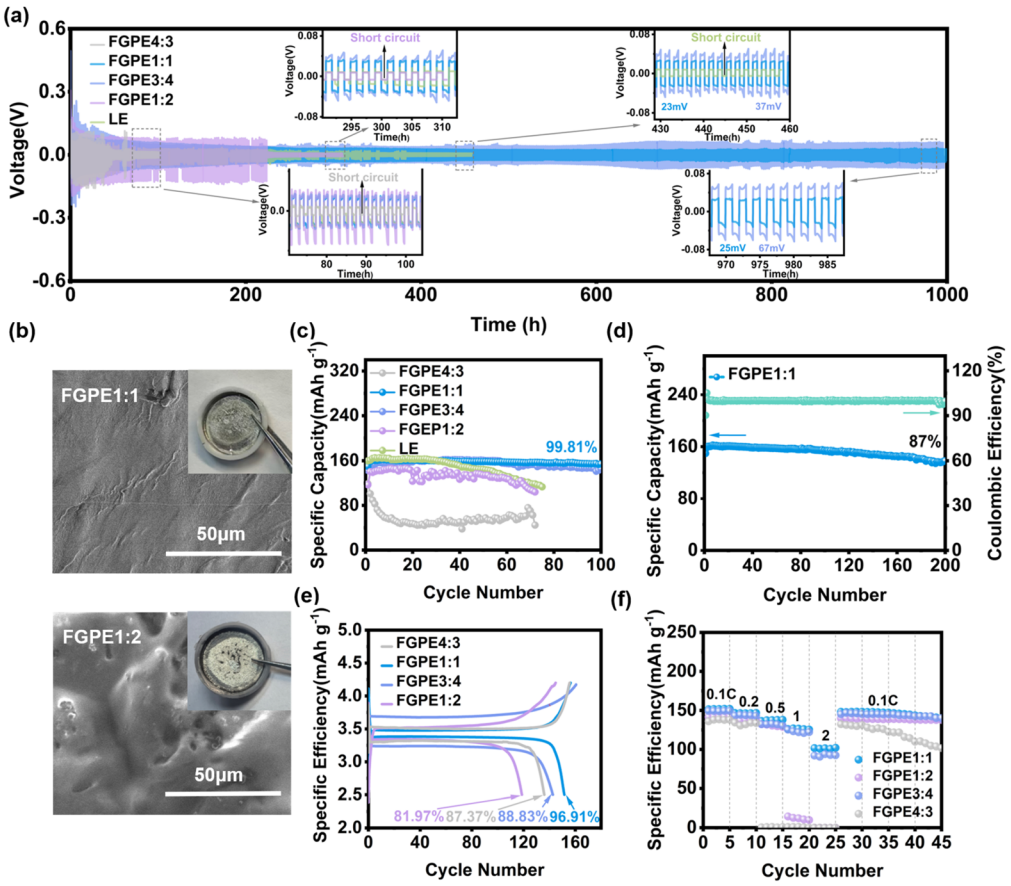

Fig. 2 (a) Polarization voltage curves of Li||Li symmetric cells with different electrolytes at a current density of 0.1 mA cm^{-2} and a capacity of 0.1 mA h cm^{-2}. (b) SEM images of LM of Li||FGPE1:1||Li and Li||FGPE1:2||Li after 100 h at a current density of 0.1 mA cm^{-2} with a capacity of 0.1 mA h cm^{-2}. (c) Cycling performance of LFP||Li cells with different electrolytes after 100 cycles at 0.2C. (d) Cycling performance of the LFP||FGPE1:1||Li cell at 0.2C. (e) Charge and discharge curves of LFP||FGPE1:1||Li at 0.2C. (f) Rate performance of LFP||Li cells with different electrolytes.

coulombic efficiency, as evidenced by the charge–discharge profiles (Fig. 2e). This improvement is attributed to a higher content of free AM, which enhances mechanical properties *via* NH_2^-rich groups, albeit with a slight penalty in Li^+ transport.[41] In contrast, excessive free HFA promotes SEI side reactions, leading to irreversible Li^+ loss. Rate capability tests (Fig. 2f) demonstrated the superior performance of FGPE1:1, delivering reversible capacities of 151.4 mA h g^{-1} (0.1C), 146.7 mA h g^{-1} (0.2C), 136.47 mA h g^{-1} (0.5C), 126.17 mA h g^{-1} (1C), and 101.66 mA h g^{-1} (2C), with 148.23 mA h g^{-1} upon returning to 0.1C, confirming excellent rate recovery.

Electrochemical impedance spectroscopy (EIS) and temperature-dependent ionic conductivity measurements (Fig. 3a and S8a) show that FGPE1:1 reached the highest ionic conductivity (1.21 mS cm^{-1}) at 25 °C among FGPEs, which also reveal that increasing free HFA content reduces ionic conductivity due to fluorine-induced intermolecular repulsion.[42] Arrhenius analysis (Fig. 3b) further demonstrates the lower activation energy of FGPE1:1 (15.19 kJ mol^{-1} *vs.* 22.16 kJ mol^{-1} for LE), suggesting facilitated Li^+ migration. Thermogravimetric analysis (Fig. 3c) highlights FGPE1:1's exceptional thermal stability, with only 2% mass loss at 100 °C and 46% at 200 °C, outperforming LE (47% loss at 100 °C) and other FGPEs. This improved thermal resistance is attributed to the effective confinement of organic solvents and LiFSI within the gel network. Differential scanning calorimetry (DSC) results (Fig. S8b) confirm the amorphous nature of FGPE1:1 ($T_g = 182.5$ °C), which, combined with its anion-rich solvation structure, enables a wide electrochemical stability window (4.75 V *vs.* 4.2 V for LE, Fig. 3d and S8c).[43] The Li^+ transport kinetics at the electrolyte/electrode interface were evaluated using exchange current densities derived from Tafel plots (Fig. S8h). Over the voltage range of −0.2 to 0.2 V, FGPE1:1 exhibits the highest exchange current density (0.070 mA cm^{-2}), indicating that the SEI formed at the FGPE1:1/Li interface has the lowest Li^+ transport resistance. Chronoamperometry (CA) and EIS

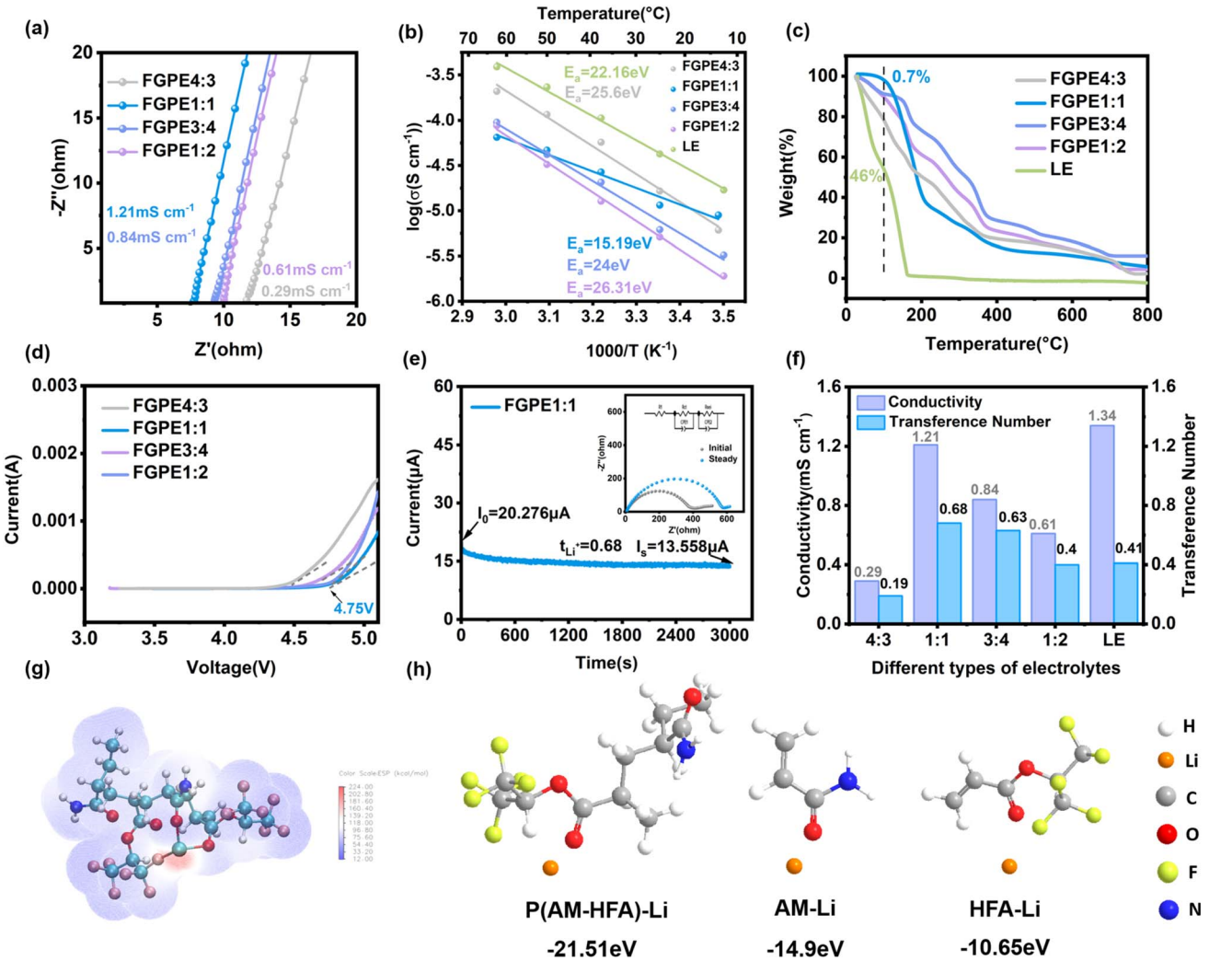

Fig. 3 (a) The ionic conductivity of FGPEs at varying ratios was measured at 25 °C. (b) Relationship between σ and temperature for FGPEs and LE. (c) TGA curves of the LE and FGPEs under N_2 flow at a heat rate of 10 °C min^{-1}. (d) Linear sweep cyclic curves of FGPEs. (e) Current densities and EIS curves of Li||FGPE1:1||Li before and after polarization. (f) The room-temperature ionic conductivity and lithium-ion transference number of different types of electrolytes. (g) ESP maps of P(AM-HFA). (h) DFT calculation of Li^+ absorption energy for P(AM-HFA) and monomers.

measurements (Fig. 3e) reveal the high t_{Li^+} of FGPE1:1 (0.68 *vs.* 0.41 for LE, Fig. S8f), underscoring its ability to mitigate concentration polarization through coordinated ion-hopping mechanisms. To investigate coordination between the polymer and Li^+, density functional theory (DFT) calculations were performed to map the electrostatic potential (ESP) distribution and to compute the binding energies of polymer–Li^+ and free monomer–Li^+ complexes. The ESP maps (Fig. 3g) show distinct regions of negative and positive potential that guide coordination between electron-rich sites and Li^+. Notably, the P(AM-HFA) isosurface displays pronounced negative ESP (red) around the C=O and C–F groups, consistent with Lewis base coordination to Li^+.[31] Compared with the C–F group (dipole moment 4.64×10^{-30} C m),[44] the stronger dipole moment of the C=O group (7.7×10^{-30} C m) more effectively promotes lithium salt dissociation *via* enhanced ion–dipole interactions with Li^+, thereby generating more freely mobile Li^+ ions. As shown in Fig. 3h, the copolymer P(AM-HFA) exhibits a substantially more favorable (more negative) Li^+ binding energy (−21.51 eV) than the free AM (−14.9 eV) and HFA (−10.65 eV) moieties, suggesting a cooperative effect in which AM provides strong C=O dipoles and HFA contributes C–F groups to enhance salt dissociation and facilitate Li^+ transport.[25] Unlike other FGPEs, where excess free monomers hinder ion mobility, the high fraction of P(AM-HFA) in FGPE1:1 minimizes such interference and yields a higher Li^+ transference number, consistent with Fig. 3f. Comparative analysis (Fig. 3f and S8d–g) confirms FGPE1:1's optimal balance of t_{Li^+} and ionic conductivity (σ). Despite exhibiting a slightly lower ionic conductivity (1.21×10^{-3} S cm^{-1} at 25 °C) than the liquid electrolyte (LE, 1.34×10^{-3} S cm^{-1}), FGPE1:1 demonstrates a markedly higher Li^+ transference number (t_{Li^+}), indicating enhanced Li^+ transport through the polymer matrix. The polymer framework's restriction of anion mobility enhances Li^+ transport while ensuring stability across a broad temperature range.[45] These properties, coupled with superior thermal, electrochemical, and dendrite-suppression performance, establish FGPE1:1 as a promising electrolyte for high-performance lithium metal batteries.

X-ray photoelectron spectroscopy (XPS) depth profiling was utilized to investigate the SEI composition on lithium anodes after 100 hours of cycling in symmetric cells (Fig. 4a–c). The F 1s spectrum (Fig. 4a) reveals the formation of polymer-modified LiF, originating from both FEC decomposition and fluorinated polymer–lithium interactions.[27] Notably, the LiF concentration increases with etching depth, while C–F species decrease, indicating the protective role of FGPE1:1 in stabilizing the cycling process. The C 1s spectrum (Fig. 4b) shows characteristic peaks corresponding to C–O and C=O bonds (solvent/salt decomposition) and –$CONH_2$ (polymer amide groups, Fig. S9j).[46] The intensity of C-related peaks diminishes with etching depth, suggesting a decrease in organic species and an increase in inorganic components (*e.g.*, Li_2CO_3) in the inner SEI, which effectively suppresses lithium dendrite growth. The Li 1s spectrum (Fig. 4c) demonstrates depth-dependent variations: inorganic components (LiF, Li_2CO_3) dominate near the lithium interface, while organic –CO–O–Li species are more prevalent at the SEI surface. Furthermore, we compared the XPS spectra of SEI surfaces formed after 100 h of cycling at 0.1 mA cm^{-2} with an areal capacity of 0.1 mA h cm^{-2} using FGPE1:1 and LE (Fig. S9a–f). The F 1s and C 1s spectra for FGPE1:1 (Fig. S9a and b) show substantial C–F species originating from the fluorinated polymer electrolyte. In LE, the F 1s peak at 684.1 eV is assigned to SO_2F_y species from LiFSI decomposition (Fig. S9d).[47] In both electrolytes, the F 1s peak at 684.9 eV corresponds to LiF formed by minor decomposition of FEC. The polymer-electrolyte-modified Li surface also shows a small amount of R–CO–OLi species (Fig. S9c and f). These findings collectively show that fluorinated polymer modification promotes an inorganic-rich SEI (LiF/Li_2CO_3) at the lithium interface (Fig. 4d), effectively protecting the metal anode. This is further corroborated by the superior coulombic efficiency of FGPE1:1 (92.78% *vs.* LE's 62.77% over 10 cycles, Fig. S7e), indicating enhanced interfacial stability.

The composition of the CEI layers in FGPE1:1 and LE was further characterized by XPS (Fig. 4e, f and S9g–j). The F 1s spectrum (Fig. 4e) shows components corresponding to LiF (684.7 eV) and C–F (688 eV). Fig. 4e and S9g demonstrate an increased LiF abundance in cycled FGPE1:1, suggesting enhanced involvement of FSI^- in the compositional formation of CEI. The LiF-rich interface, with its low Li^+ diffusion barrier (10^{-31} S cm^{-1}) and high surface energy,[34] promotes uniform Li deposition and effectively suppresses electrolyte decomposition by blocking electron transfer.[48] The C 1s spectrum (Fig. 4f) exhibits components at 289.3 eV (CO_3^{2-}), 288.4 eV (C=O), 286.8 eV (C–O), and 284.8 eV (C–C/C–H). Relative to LE (Fig. S9h), the polymer electrolyte promotes greater Li_2CO_3 formation at the cathode, reinforcing the CEI and yielding a more robust, conductive interface that improves cycling stability and rate performance. The N 1s spectrum (Fig. S9j) is dominated by –CO–NH_2 (399.9 eV) and –NH_2 (398.2 eV) signals from the polymer electrolyte, whereas in LE (Fig. S9i) the N 1s signal mainly arises from LiFSI decomposition products. TEM imaging confirms the presence of an ultrathin (∼8 nm) homogeneous CEI layer (Fig. 4g), which ensures stable operation within the voltage range of 2.5–4.2 V. Notably, the fluorinated polymer electrolyte exhibits exceptional safety characteristics, showing no combustion after 2 seconds in flammability tests (Fig. 4i). Practical validation was achieved through a 3.4 V pouch cell that successfully powered an LED panel (Fig. 4h), demonstrating its practical applicability. Post-cycling analysis (Fig. S10) confirms the structural integrity of LFP particles, further highlighting the compatibility between FGPE1:1 and the cathode materials.

In summary, we successfully synthesized fluorine-grafted gel polymer electrolytes (FGPEs) *via in situ* polymerization. At an optimal AM/HFA molar ratio of 1 : 1, the coordination between Li^+ ions and oxygen atoms in the electrolyte is effectively suppressed. Additionally, a multi-functional polymer network is utilized, incorporating –C=O and C–F groups to establish fast Li^+ transport channels and secondary amine (–NH_2) groups to anchor anions, thereby promoting ion transport.[49,50] As a result, the *in situ* prepared FGPE1:1 exhibits satisfactory ionic conductivity (σ = 1.21 mS cm^{-1}) and Li^+ transference number (t_{Li^+} = 0.68) at 25 °C, respectively. By integrating strong dipole functional groups (C=O and C–F) with the flexible solvent DME, this

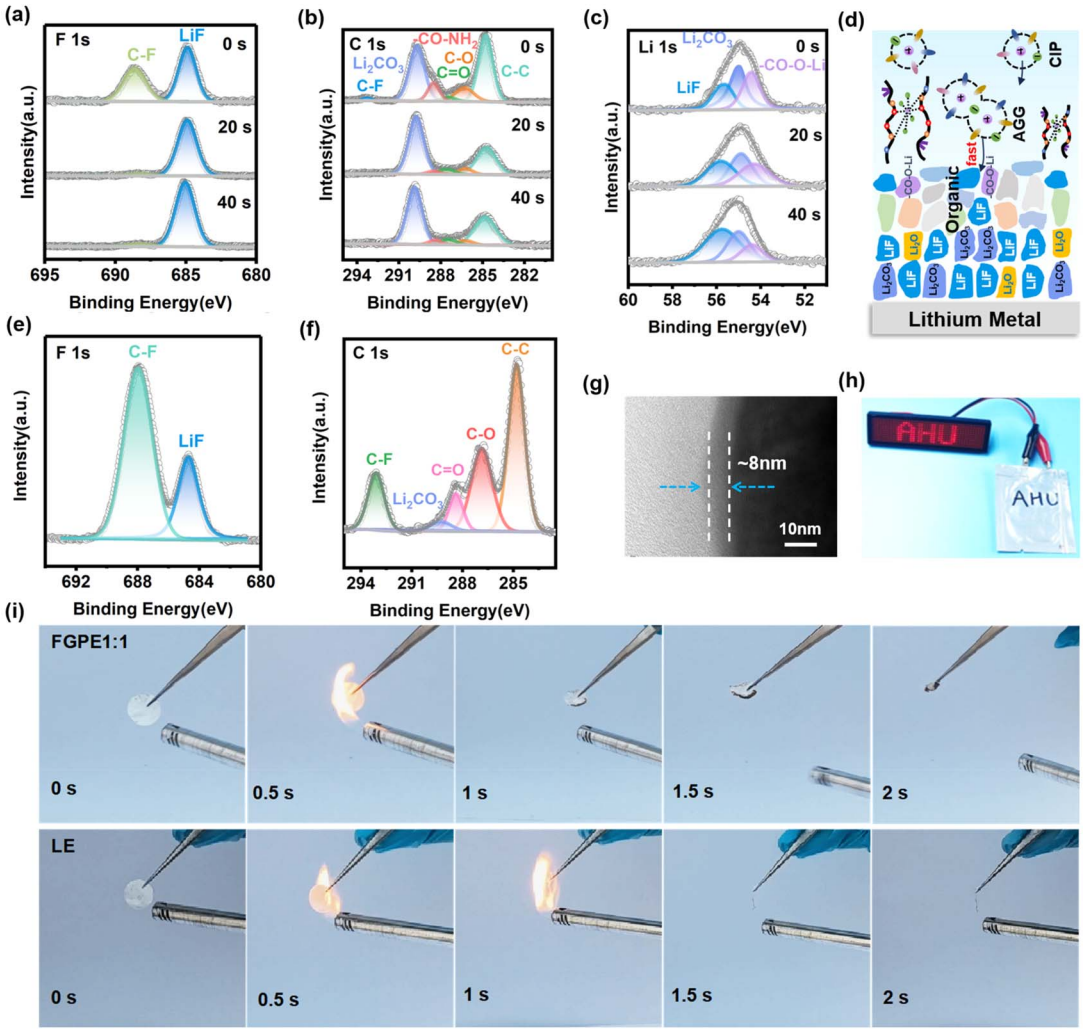

Fig. 4 (a–c) XPS depth profiles of C 1s, O 1s, Li 1s, and F 1s in the lithium metal anode cycled in Li||Li cells with FGPE1:1. (d) Schematic diagram of the chemical composition distribution on the SEI film surface. (e and f) The XPS depth spectra for F 1s and C 1s of the LFP cathode surface after 100 cycles of LFP||FGPE1:1||Li at 0.2C. (g) The transmission electron microscopy (TEM) characterisation of the cathode surface in the LFP||FGPE1:1||Li cell following 110 cycles at 0.2C. (h) LFP||FGPE1:1||Li pouch cell lit LEDs under ambient temperature conditions. (i) Combustion tests of FGPE1:1 and LE.

copolymer system synergistically tailors the solvation structure of Li^+ at the molecular level, enabling efficient ion dissociation and low-energy-barrier transport.[51–53] Furthermore, weak solvation of Li^+ and the introduction of abundant C–F result in the formation of inorganic-rich interphase layers on both cathode and anode surfaces, which effectively suppresses interfacial side reactions and preserves electrode integrity.[39] Consequently, the full cell assembled with FGPE1:1 demonstrates stable cycling over 200 cycles at 0.2C within a voltage range of 2.5–4.2 V, with a capacity retention of 87%. Even at 1C, it delivers a high discharge capacity of 126.17 mA h g^{-1}. This work provides novel insights into the design of polymer electrolytes for stable and highly conductive lithium metal batteries.

Author contributions

J. G. designed the experiments, prepared the materials, conducted the electrochemical measurements and performed writing of the original draft and formal analysis; Y. Z. provided assistance with additional formal analysis; C. Y. supported review, editing and investigation; D. K. and Z. J. contributed to creating the flowchart image; Y. L. supported data curation and DFT calculations; Q. W., X. Z. and T. Z. conceived the project, and provided guidance and supervision throughout the work. All authors have approved the final version of the manuscript.

Conflicts of interest

There are no conflicts to declare.

Data availability

The data supporting this article have been included as part of the SI. Supplementary information includes Fig. S1–S10, which provide additional experimental results, electrochemical data

analysis, and supporting evidence referenced throughout the main text. See DOI: https://doi.org/10.1039/d5sc05270j.

Acknowledgements

This work was supported by the Anhui Provincial Natural Science Foundation for Outstanding Young Scholar (2208085Y05), the Anhui Provincial Scientific Reuter Foundation for Returned Scholars (2022LCX030) and Anhui Province Graduate Education Quality Project (2024XSCX030).

Notes and references

1 S. Zhang, R. Li, T. Deng, Q. Ma, X. Hong, H. Zhang, R. Zhang, S. Ding, Y. Wu, H. Zhu, M. Li, H. Zhang, D. Lu, B. Ma, L. Lv, Y. Li, L. Chen, Y. Shen, R. Guo and X. Fan, *Nat. Energy*, 2024, **9**, 1285–1296.
2 C. Yang, Z. Jiang, X. Chen, W. Luo, T. Zhou and J. Yang, *Chem. Commun.*, 2024, **60**, 10245–10264.
3 Q. Lu, C. Yang, Y. Xu, Z. Jiang, D. Ke, R. Meng, S. Hu, Y. Chen, C. Zhang, J. Yang and T. Zhou, *Chem. Sci.*, 2024, **16**, 1791–1801.
4 P. Wang, X. Dai, P. Xu, S. Hu, X. Xiong, K. Zou, S. Guo, J. Sun, C. Zhang, Y. Liu, T. Zhou and Y. Chen, *eScience*, 2023, **3**, 100088.
5 Q. Wang, H. Wang, J. Wu, M. Zhou, W. Liu and H. Zhou, *Nano Energy*, 2021, **80**, 105516.
6 Q. Zhao, S. Stalin and L. A. Archer, *Joule*, 2021, **5**, 1119–1142.
7 H. Wang, L. Sheng, G. Yasin, L. Wang, H. Xu and X. He, *Energy Storage Mater.*, 2020, **33**, 188–215.
8 Q. Huang, J. Song, Y. Gao, D. Wang, S. Liu, S. Peng, C. Usher, A. Goliaszewski and D. Wang, *Nat. Commun.*, 2019, **10**, 1–7.
9 Z. Lin, S. Liu, C. Cui, W. Liu, Y. Su, H. Song, L. Du, J. Hu and Z. Cui, *Sci. China. Chem.*, 2025, **68**, 1–22.
10 H. Xu, S. Yang and B. Li, *Adv. Energy Mater.*, 2024, **14**, 2303539.
11 J. Qiu, X. Liu, R. Chen, Q. Li, Y. Wang, P. Chen, L. Gan, S. J. Lee, D. Nordlund, Y. Liu, X. Yu, X. Bai, H. Li and Y. Chen, *Adv. Funct. Mater.*, 2020, **30**, 1909392.
12 Y. Ma, R. Zhang, L. Wang, J. Wu, B. Chen, Y. Yu, L. Li, F. He, C. Shi, N. Zhao, C. He and A. B. Wong, *Energy Storage Mater.*, 2023, **61**, 1028936.
13 J. Liu, T. You, Y. Zhao, F. Liu, J. Li, L. Wang, C. Wang and L. Li, *Rare Met.*, 2025, **44**, 3817–3826.
14 H. Li, R. Hua, Y. Xu, D. Ke, C. Yang, Q. Ma, L. Zhang, T. Zhou and C. Zhang, *Chem. Sci.*, 2023, **14**, 10147–10154.
15 X. Miao, J. Hong, S. Huang, C. Huang, Y. Liu, M. Liu, Q. Zhang and H. Jin, *Adv. Funct. Mater.*, 2025, **35**, 2411751.
16 Z. Deng, S. Chen, K. Yang, Y. Song, S. Xue, X. Yao, L. Yang and F. Pan, *Adv. Mater.*, 2024, **36**, 2407923.
17 S. Peng, J. Fu, L. Wei and X. Guo, *Chem. Commun.*, 2025, **61**, 868–880.
18 T. Agnihotri, S. A. Ahmed, E. B. Tamilarasan, R. Hasan, W. Su and B. J. Hwang, *Adv. Funct. Mater.*, 2023, **34**, 2311215.
19 X. Deng, J. Chen, X. Jia, X. Da, Y. Zhao, Y. Gao, Y. Gao, X. Kong, S. Ding and G. Gao, *Angew. Chem., Int. Ed.*, 2024, **136**, e202410818.
20 A. Tang, E. Hu, B. Jia, C. Wan, Z. Wen, S. Tso, X. Ju and Q. Yan, *Rare Met.*, 2025, **44**, 2268–2293.
21 G. Wang, Q. Ma, T. Zhang, Y. Deng and G. Zhang, *Nano Energy*, 2025, **140**, 111064.
22 C. Liu, F. Zhu, Z. Huang, W. Liao, X. Guan, Y. Li, D. Chen and Z. Lu, *Chem. Eng. J.*, 2022, **434**, 134644.
23 B. Zhang, Y. Wu, Y. Hou, J. Chen, Z. Ma and D. Zhao, *Small*, 2024, **20**, 2305322.
24 S. Zhang, B. Xie, X. Zhuang, S. Wang, L. Qiao, S. Dong, J. Ma, Q. Zhou, H. Zhang, J. Zhang, J. Ju, G. Xu, Z. Cui and G. Cui, *Adv. Funct. Mater.*, 2024, **34**, 2314063.
25 X. Zheng, S. Ma, Y. Zhang, W. Lin, K. Ji, C. Wang and M. Chen, *Macromolecules*, 2023, **56**, 1077–1085.
26 J. Huang, Z. Shen, S. J. Robertson, Y. Lin, J. Zhu, K. Yang, Y. Wang, M. Shao and Z. Shi, *Chem. Eng. J.*, 2023, **475**, 145802.
27 J. Luo, Q. Huang, D. Shi, Y. Qiu, X. Zheng, S. Yang, B. Li, J. Weng, M. Wu, Z. Liu, Y. Yu and C. Yang, *Adv. Funct. Mater.*, 2024, **34**, 2403021.
28 Y. Wang, Z. Wang, Y. Zhao, X. Yang, J. Xu, X. Ye, X. Jiang, Y. Chen, C. Li and D. Ye, *J. Power Sources*, 2024, **593**, 233881.
29 X. Song, J. Sun, W. Ren, L. Wang, B. Yang, H. Ning, P. Zhang, Z. Caixiang, Z. Tie, X. Zhang, Y. NuLi and Z. Jin, *Angew. Chem., Int. Ed.*, 2025, **64**, e202417450.
30 C. Luo, Q. Liu, X. Wang, Y. Tian, Z. Liu, F. Kang and B. Li, *Nano Energy*, 2023, **109**, 108323.
31 Y. Zhang, T. Cheng, S. Gao, H. Ding, Z. Li, L. Li, D. Yang, H. Yang and P. F. Cao, *Mater. Horiz.*, 2025, **12**, 1189–1199.
32 K. Mu, W. Dong, W. Xu, Z. Song, R. Wang, L. Wu, H. Li, Q. Liu, C. Zhu, J. Xu and L. Tian, *Adv. Funct. Mater.*, 2024, **34**, 2405969.
33 D. Zhang, Y. Liu, D. Li, S. Li, Q. Xiong, Z. Huang, S. Wang, H. Hong, J. Zhu, H. Lv and C. Zhi, *Energy Environ. Sci.*, 2025, **18**, 227–235.
34 W. Min, L. Li, M. Wang, S. Ma, H. Feng, W. Wang, H. Ding, T. Cheng, Z. Li, T. Saito, H. Yang and P. Cao, *Angew. Chem., Int. Ed.*, 2025, **64**, e202422510.
35 M. Zhou, W. Chen, H. Yang, Y. Hu, T. Lei, D. Chen, S. Wang, Y. Zhang and J. Xiong, *Adv. Energy Mater.*, 2024, **15**, 2403082.
36 G. Hu, Z. Xu and Z. Wang, *Chem. Commun.*, 2025, **61**, 4852–4855.
37 Z. Zhao, G. Melinte, D. Guo, Y. Lei, M. N. Hedhili, X. Guo, Z. Shi, Y. Wang, J. K. El-Demellawi, W. Zhao and H. N. Alshareef, *Energy Environ. Sci.*, 2025, **18**, 2826–2838.
38 L. Wu, F. Pei, D. Cheng, Y. Zhang, H. Cheng, K. Huang, L. Yuan, Z. Li, H. Xu and Y. Huang, *Adv. Funct. Mater.*, 2024, **34**, 2310084.
39 Y. Liu, Z. Jin, Z. Liu, H. Xu, F. Sun, X. Q. Zhang, T. Chen and C. Wang, *Angew. Chem., Int. Ed.*, 2024, **136**, e202405802.
40 H. Tu, L. Li, Y. Hu, Y. Zhang, Y. Wang, W. Huang, Z. Ren, H. Lin and M. Liu, *Chem. Eng. J.*, 2022, **434**, 134647.
41 J. Luo, Q. Huang, D. Shi, Y. Qiu, X. Zheng, S. Yang, B. Li, J. Weng, M. Wu, Z. Liu, Y. Yu and C. Yang, *Adv. Funct. Mater.*, 2024, **34**, 2403021.
42 N. Xu, Y. Zhao, M. Ni, J. Zhu, X. Song, X. Bi, J. Zhang, H. Zhang, Y. Ma, C. Li and Y. Chen, *Angew. Chem., Int. Ed.*, 2024, **63**, e202404400.

43 W. Song, B. Li, Y. Qu, W. Jiang, M. Pei, N. Hu, S. Zhuo, C. Su, X. Jin, R. Mao, D. Liu, X. Jian and F. Hu, *Angew. Chem., Int. Ed.*, 2025, **64**, e202505095.
44 D. Zhang, Z. Luo, H. Xu, Y. Guo, H. Chen, Y. Ye, J. An, J. Hui, Y. Shi, S. Yang and B. Li, *Adv. Funct. Mater.*, 2024, **34**, 2409134.
45 S. Qin, M. Wu, H. Zhao, J. Li, M. Yan, Y. Ren and Y. Qi, *J. Mater. Sci. Technol.*, 2024, **199**, 197–205.
46 S. Chai, Y. Zhang, Y. Wang, Q. He, S. Zhou and A. Pan, *eScience*, 2022, **2**, 494–508.
47 Y. Zhao, T. Zhou, L. P. Jeurgens, X. Kong, J. W. Choi and A. Coskun, *Chem*, 2023, **9**, 682–697.
48 J. Park, H. Seong, C. Yuk, D. Lee, Y. Byun, E. Lee, W. Lee and B. J. Kim, *Adv. Mater.*, 2024, **36**, 2403191.
49 X. Chen, L. Yi, J. Liu, Z. Luo, Y. Shen and X. Wang, *J. Power Sources*, 2024, **603**, 234433.
50 Y. Lu, X. Zhang, Y. Wu, H. Cheng and Y. Lu, *Ind. Chem. Mater.*, 2025, **3**, 151–177.
51 L. Chen, T. Gu, J. Mi, Y. Li, K. Yang, J. Ma, X. An, Y. Jiang, D. Zhang, X. Chen, S. Guo, Z. Han, T. Hou, Y. Cao, M. Liu, W. Lv, Y. He and F. Kang, *Nat. Commun.*, 2025, **16**, 3517.
52 Z. Jiang, X. Zhang, J. Ruan, J. Zhou, Y. Yue, X. Zhou, Y. Chen, C. Zhang, Y. Li and T. Zhou, *Adv. Funct. Mater.*, 2025, **35**, e14453.
53 Q. Wang, J. Gan, Y. Zhao, C. Yang, G. Zhu, N. Wang, C. Zhang, J. Yang and T. Zhou, *EES Batteries*, 2025, **1**, 672–691.